

Article

Total Harmonic Distortion Reduction in Multilevel Inverters through the Utilization of the Moth–Flame Optimization Algorithm

Adolfo R. Lopez ^{1,†} , Oscar A. López-Núñez ^{2,†} , Ricardo Pérez-Zúñiga ^{3,†} , Jair Gómez Radilla ^{4,†},
Mario Martínez-García ^{4,†} , Maria A. López-Osorio ^{5,†}, Gerardo Ortiz-Torres ^{4,†} , Mayra G. Mena-Enriquez ^{6,†} ,
Moises Ramos-Martinez ^{4,†} , Juan Carlos Mixteco-Sánchez ^{5,†} , Carlos Alberto Torres-Cantero ^{7,8,†} ,
Felipe D. J. Sorcia-Vázquez ^{4,*,†}  and Jesse Y. Rumbo-Morales ^{4,†} 

¹ TecNM/ITS Irapuato, Irapuato 36821, Mexico; adolfo.ln@irapuato.tecnm.mx

² Facultad de Ingeniería, Universidad Autónoma de Baja California, Blvd. Benito Juárez S/N, Mexicali 21280, Mexico; oscar.lopez.nunez@uabc.edu.mx

³ Sistema de Universidad Virtual, Universidad de Guadalajara, Av Enrique Díaz de León Sur 782, Moderna, Guadalajara 44200, Jalisco, Mexico; perezuniga@udgvirtual.udg.mx

⁴ Centro Universitario de los Valles, Universidad de Guadalajara, Carretera Guadalajara-Ameca Km 45.5, Ameca 46600, Mexico; gr_jair@hotmail.com (J.G.R.); mario.mgarcia@academicos.udg.mx (M.M.-G.); gerardo.ortiztorres@academicos.udg.mx (G.O.-T.); moises.ramos@valles.udg.mx (M.R.-M.); jesse.rumbo@academicos.udg.mx (J.Y.R.-M.)

⁵ Natural and Exact Sciences Department, University of Guadalajara, Ameca 46600, Mexico; maria.osorio@academicos.udg.mx (M.A.L.-O.); juan.mixteco@academicos.udg.mx (J.C.M.-S.)

⁶ Biomedical Sciences Department, University of Guadalajara, Tonalá 45425, Mexico; guadalupe.mena@academicos.udg.mx

⁷ Tecnológico Nacional de México Campus Colima, Av. Tecnológico # 1, Col. Liberación, Villa de Álvarez 28976, Mexico; atorres@colima.tecnm.mx or cantero@ucol.mx

⁸ Facultad de Ingeniería Mecánica y Eléctrica, Universidad de Colima, Carretera Colima, Coquimatlan Km 9, Valle de las Huertas, Coquimatlán 28400, Mexico

* Correspondence: felipe.sorcia@academicos.udg.mx

† These authors contributed equally to this work.



Citation: Lopez, A.R.; López-Núñez, O.A.; Pérez-Zúñiga, R.; Gómez Radilla, J.; Martínez-García, M.; López-Osorio, M.A.; Ortiz-Torres, G.; Mena-Enriquez, M.G.; Ramos-Martinez, M.; Mixteco-Sánchez, J.C.; et al. Total Harmonic Distortion Reduction in Multilevel Inverters through the Utilization of the Moth–Flame Optimization Algorithm. *Appl. Sci.* **2023**, *13*, 12060. <https://doi.org/10.3390/app132112060>

Academic Editor: Gang Lei

Received: 14 September 2023

Revised: 30 October 2023

Accepted: 31 October 2023

Published: 5 November 2023



Copyright: © 2023 by the authors. Licensee MDPI, Basel, Switzerland. This article is an open access article distributed under the terms and conditions of the Creative Commons Attribution (CC BY) license (<https://creativecommons.org/licenses/by/4.0/>).

Abstract: This paper shows the implementation of the Moth–Flame Optimization algorithm in a Cascade-H multilevel inverter with five and seven levels to determine the optimal switching sequence of the inverter’s semiconductor devices. The algorithm was coded in Matlab software, and the obtained switching sequences were implemented in a Cascade-H multilevel inverter laboratory prototype, where the output voltage waveform was obtained using a digital oscilloscope. The experimental Total Harmonic Distortion was obtained using a power quality analyzer. The experimental results show the improvement of the Total Harmonic Distortion in the voltage output. These results were compared with other papers in the literature with different metaheuristic methods concerning the same modulation. These findings demonstrate the feasibility of employing the Moth–Flame Optimization Algorithm to significantly reduce the Total Harmonic Distortion, obtaining a lower value than most analyzed papers.

Keywords: total harmonic distortion; multilevel inverter; metaheuristic optimization methods; moth–flame optimization

1. Introduction

In recent times, there has been a growing adoption of multilevel inverters within renewable energy setups. This is primarily attributed to their qualities such as minimal common-mode voltage, reduced distortion in the input current, and the potential to incorporate semiconductors with lower switching frequencies [1,2]. The resultant voltage from a multilevel inverter takes the form of a stepped waveform, achieved through a suitable

sequence of the semiconductor switches within the inverter structure [3–5]. However, a poor sequence of the multilevel inverter semiconductors leads to a high level of THD in the output voltage. Due to the above, a well-suited arrangement of semiconductors can generate a seamless output voltage featuring minimal total harmonic distortion (THD) [6–10]. The sequence of the semiconductors can be mainly established using digital platforms, like microcontrollers or Digital Signal Processors, among others.

Numerous articles have tackled the optimization of the THD for the output voltage in the Cascade H-Bridge Multilevel Inverter Topology (CHBMLI) by obtaining and implementing the switching angles that generate the voltage output waveform by using low-frequency modulation [11–16]. The obtention of the switching angles is primarily carried out using Selective Harmonic Elimination (SHE) and the Optimal Minimization of the Total Harmonic Distortion (OMTHD).

In the SHE method, the objective is to reduce the low-order harmonics of the CHBMLI, like the 3rd, 5th, and 7th, among others [12]. This method solves a set of nonlinear equations, which are as follows:

$$\cos(\theta_1) + \cos(\theta_2) + \dots + \cos(\theta_s) = r \quad (1)$$

$$\cos(3\theta_1) + \cos(3\theta_2) + \dots + \cos(3\theta_s) = 0 \quad (2)$$

$$\cos(5\theta_1) + \cos(5\theta_2) + \dots + \cos(5\theta_s) = 0 \quad (3)$$

$$\vdots$$

$$\cos(n\theta_1) + \cos(n\theta_2) + \dots + \cos(n\theta_s) = 0 \quad (4)$$

In this context, r represents the magnitude of the fundamental value that has been suggested. The Equations (2) to (4) need to be equated to zero to remove the contribution of that specific harmonic, thus yielding the correct switching angles for the semiconductor devices. Therefore, reducing or eliminating the low-order harmonics using this method achieves a low THD value. These equations also need to satisfy the following condition: $0 \leq \theta_1 \leq \theta_2 \dots \leq \theta_n \leq \frac{\pi}{2}$, where $0 \leq \theta_1$ to $0 \leq \theta_n$ represents the switching angles of the CHBMLI.

To address Equations (2) to (4), numerous authors employ metaheuristic algorithms, which mimic the advantageous characteristics found in nature, driven by the principles of natural selection and societal adaptation [17]; for instance, the SHE method, along with the Genetic algorithm (GA), is used in reference [18] to eliminate the 5th and 7th harmonics in a seven-level CHBMLI, while the authors of reference [19] use the Newton Raphson (NR) and the Particle Swarm Optimization (PSO) algorithm to eliminate the 5th and 7th harmonics as well in a seven-level CHBMLI. By contrast, in reference [20], this method is simulated to eliminate the odd harmonics up to the 15th with the GA algorithm.

On the other hand, the OMTHD technique also allows for obtaining the switching angles of a CHBMLI; however, the objective of this function is to directly reduce the THD in the output voltage pattern of a CHBMLI, and, compared to the SHE method, the OMTHD manipulates the value of the harmonics without maintaining or eliminating any specific harmonics (including the fundamental component) [11].

The OMTHD method has been carried out using conventional techniques like the NR method [11,15], where the authors obtained the THD values for the CHBMLI across configurations of five, seven, and nine levels. However, many authors have been using metaheuristic algorithms just as in the SHE method. For instance, in reference [15], a comparison is made between the THD by applying Particle Swarm Optimization (PSO), showing a good performance of this algorithm, but only simulation results are shown.

In reference [14], the authors use the PSO in a five-level multilevel CHBMLI to obtain a low THD; the results were compared with the SHE method. The authors of reference [16] achieve the minimization of the THD in a seven-level CHBMLI of three phases by using the GA; however, no experimental results were shown. In reference [13], the Artificial Bee

Colony (ABC) algorithm is explored to improve the voltage output THD in a five- and seven-level CHBMLI; the results were compared with the fsolve method included in the Matlab 2018b software.

Previous studies predominantly focused on commonly employed metaheuristic methods. Nevertheless, the present investigation identified an overlooked aspect: the absence of prior examinations of the Moth–Flame Optimization (MFO) algorithm in addressing this issue. The principal contribution of this paper lies in venturing into this uncharted territory by utilizing the MFO algorithm to enhance the Total Harmonic Distortion (THD) for both five- and seven-level configurations of a CHBMLI. This paper employs the OMTHD method for the inverter modulation, obtaining the switching sequences and excluding the consideration of the SHE method or other modulation techniques. The OMTHD algorithm was obtained using the Matlab software; these sequences were then implemented in a microcontroller that controls a laboratory prototype for the CHBMLI.

The CHBMLI prototype's THD for five and seven levels was obtained using a Power Quality Analyzer, showing the levels of the harmonics in a bar graph. These obtained THD were compared with previous studies that aimed to reduce the THD using the same objective function (OMTHD) but with different metaheuristic algorithms. The comparisons demonstrate that the MFO algorithm consistently outperforms the other algorithms by achieving lower THD values in most reported cases.

The structure of this paper is outlined in the following way: Section 2 shows the explanation of the MFO algorithm, as well as the multilevel inverter topology, and then the OMTHD objective function used for optimization is established, which includes a detailed explanation. Section 3 presents the outcomes obtained from the MFO along with the practical application of those outcomes in a laboratory prototype. The results discussion is presented in Section 4, where it can be observed that the MFO algorithm successfully obtains a low THD in both cases presented; in addition, in many cases, this algorithm demonstrates superior THD in the output voltage compared to the alternative algorithms documented in the existing literature. Lastly, Section 5 presents the conclusions.

2. Materials and Methods

2.1. Moth–Flame Optimization Algorithm

Seyedali Mirjalili introduced this nature-inspired algorithm in the year 2015. It relies on the navigation strategy utilized by moths, referred to as transverse orientation [21]. Moths employ this method for nocturnal navigation, maintaining a constant angle to the moon; this allows them to travel in a direct trajectory over extended distances [22,23]. However, when the moths find artificial lights, they become trapped in a spiral path; this occurs when the lights are exceptionally close compared to the moon [24,25]. The moths then try to keep a similar angle to the source of light, which leads to a deadly spiral fly path [22,26].

The moth acts as a search agent or particle, while the artificial light (the flame) represents a local solution. In this way, the search agent (the moth) spirals around the local solution (the flame), getting closer to it as time passes [27,28].

The MFO algorithm employs a population denoted as X , which simulates the foraging actions of N moths under the influence of simulated light. A particle x_i represents each moth, so the population is expressed as $X = \{x_1, x_2, \dots, x_N\}$.

When the MFO algorithm is initiated, the set of particles X^0 is created to form the initial population. This set of particles is defined as $X^0 = \{x_1^0, x_2^0, \dots, x_N^0\}$, and each initial particle $X_i^0 = \{x_{i,1}^0, x_{i,2}^0, \dots, x_{i,d}^0\}$ is randomly implemented within a low limit (lb) and a superior limit (ub) in the dimensional space research. Equations (5) and (6) show the initialization of the particles.

$$x_{ij}^0 = lb_j + rand_{ij}(ub_j - lb_j) \quad (5)$$

$$i = 1, 2, \dots, N; \quad j = 1, 2, \dots, d \quad (6)$$

where x_{ij}^0 is the initialization of particle i in its j dimension, the limits are shorted with lb_j and ub_j , which are the inferior and the superior limits for the j dimension, respectively. $Rand_{ij}$ is a random value corresponding to the particle i in its dimension j , whose value is in the interval $[0,1]$. At the beginning of the algorithm, the algorithm parameters are defined, such as the number of particles N , the number of dimensions d , the search station limits lb and ub , and the maximum number of iterations k_{max} .

Each particle moves in the search space by using transverse orientation; this is modeled in a logarithmic spiral s_i , which is defined as follows:

$$s_i = D_i e^{br} \cos(2\pi r) + F_j \quad (7)$$

where b is a constant representing the shape of the logarithmic spiral; in this algorithm, it has a value of 1 [29,30]. D_i represents the absolute value of the distance between the particle x_i and the local solution F_j , which is expressed as follows [31,32]:

$$D_i = |F_j - x_i| \quad (8)$$

The parameter r is a random number between -2 and 1 . It determines how close the position of the particle will be from a local solution; this value is calculated for every dimension as follows:

$$r = (a - 1) * rand + 1 \quad (9)$$

where a is a convergence constant used to emphasize exploitation as iterations progress. The defined convergence constant holds a value of

$$a = -1 + k \left(\frac{N - 1}{k_{max}} \right) \quad (10)$$

In addition to harnessing the convergence constant to facilitate a seamless transition between the exploration and exploitation stages, an additional strategic dimension comes into play within the MFO algorithm; this involves deliberately managing the number of localized solutions, often denoted as “flames”, throughout each iteration. This population of localized solutions is systematically whittled down through a gradual and calculated reduction until only a solitary solution endures. This strategic control, executed in tandem with the convergence above constant, enhances the algorithm’s convergence trajectory and bolsters its overall efficacy. The MFO algorithm navigates the intricate optimization landscape by orchestrating these multifaceted tactics, engendering enhanced precision and reliability in pursuing optimal solutions. The number of local solutions nF gradually decreases from N to 1 with the following expression [33]:

$$nF = \text{round} \left(N - k \frac{N - 1}{k_{max}} \right) \quad (11)$$

where N is the number of solutions, like other algorithms, the MFO keeps track of the best global solution g , which is the best particle (best local solution) at the moment [29]:

$$g = x_i \in \{X\} \mid f(x_i) = \min \{f(x_1), f(x_2), \dots, f(x_N)\} \quad (12)$$

Figure 1 displays the MFO algorithm flowchart, where the stop criteria is usually the number of iterations of the algorithm.

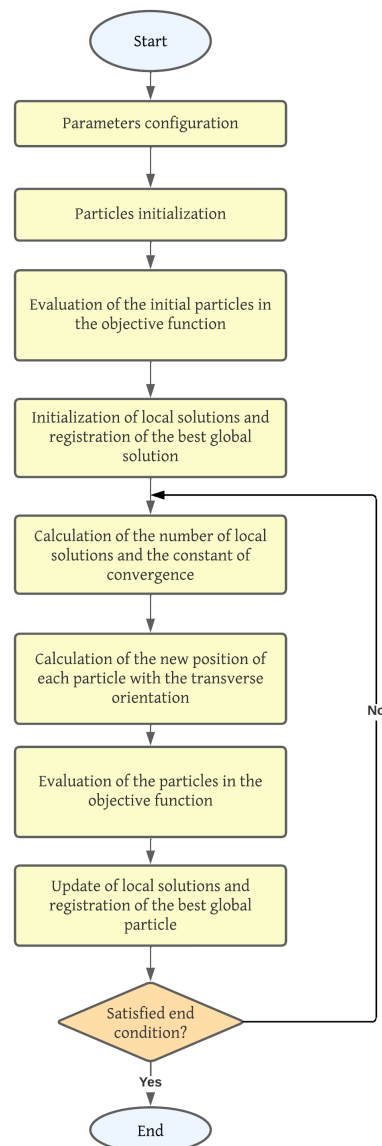


Figure 1. MFO algorithm diagram.

2.2. Multilevel Inverter Topology

Within the array of available multilevel inverter topologies, the Cascade H-Bridge Multilevel Inverter (CHBMLI) stands out by its distinctive composition, where multiple Cascade H-bridge inverters are intricately interconnected in a series configuration. This intricate arrangement amplifies the inverter's potential to generate high-quality output voltage with enhanced levels of precision and reduced harmonic distortions [34]. A distinct input voltage characterizes each inverter, and the resulting output voltage is formed by aggregating all the voltage levels generated by each inverter (Figure 2). The output voltage levels in this inverter are two times the number of the separate direct current (DC) sources plus one [35,36].

Within the diverse array of the CHBMLI modulation techniques, one exceptionally fundamental and widely employed method entails fundamental frequency switching. This intricate approach revolves around the meticulous determination of precise switching angles for the semiconductor devices. These calculated angles serve as the blueprint for the obtention of the voltage generation, explicitly targeting the creation of the fundamental voltage waveform [37,38]. However, it is worth noting that finding the switching angles requires solving nonlinear equations [35].

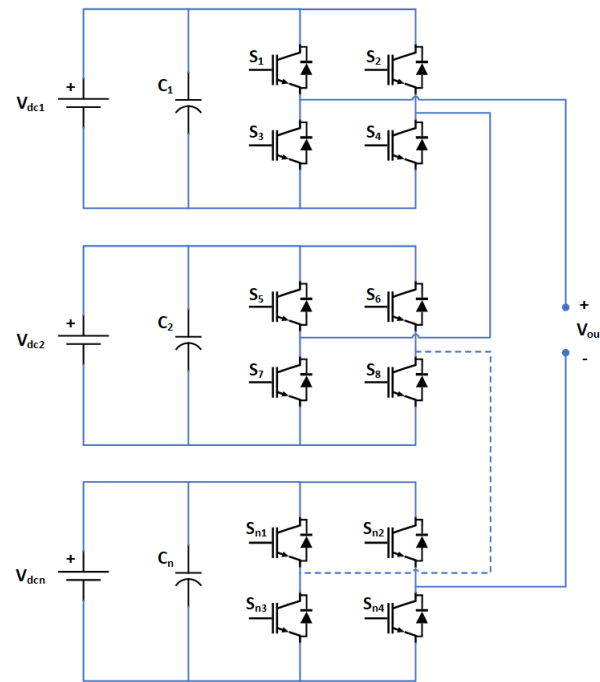


Figure 2. General CHBMLI topology.

Figure 3 shows the output voltage waveform for a five-level CHBMLI configuration to provide a visual anchor. Within this context, the critical angles that demand meticulous calculation are θ_1 and θ_2 , serving as the linchpins for shaping the desired voltage output profile. When extending our inquiry to the seven-level CHBMLI configuration, depicted in the insightful portrayal of Figure 4, the complexity deepens. Now, not only must θ_1 and θ_2 be diligently computed, but an additional angle, θ_3 , comes into play, further emphasizing the intricacy and precision required to determine these switching angles.

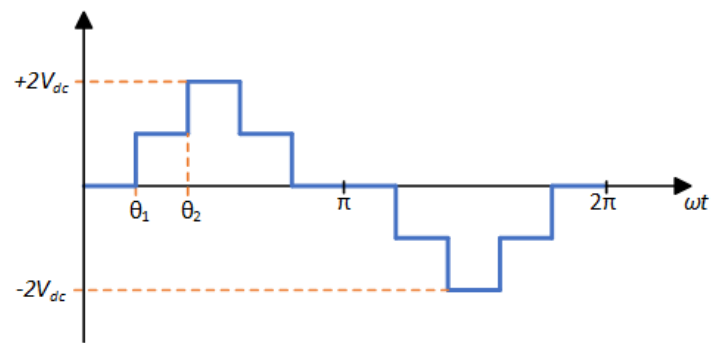


Figure 3. Five-level CHBMLI voltage.

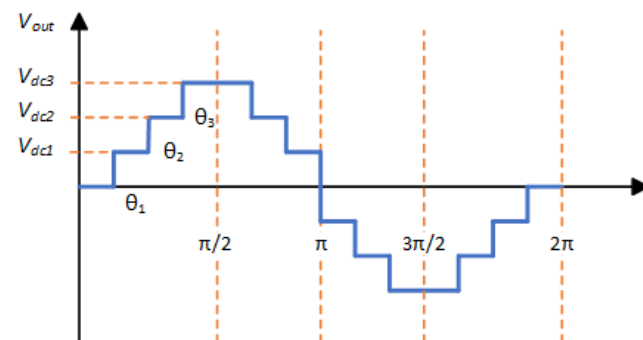


Figure 4. Seven-level CHBMLI voltage.

2.3. Problem to Optimize

The optimization problem of this paper is the reduction of the THD in a CHBMLI. The THD measures the voltage or current waveform distortion produced by the harmonics. By using the Fourier series, the output voltage waveform is examined [39]:

$$V_{out}(\omega t) = \sum_{n=1,3,5,\dots}^{\infty} \frac{4V_{dc}}{n\pi} \left[\sum_{k=1}^s \cos(n\theta_k) \right] \sin(n\omega t) \quad (13)$$

where n is the odd harmonic order; (1, 3, 5, 7, 9...);

s is the number of inverter stages;

k is an integer > 0 ;

and θ_k is the k – th switching angle.

The angles are constrained to satisfy the following:

$$0 \leq \theta_1 \leq \theta_2 \dots \leq \theta_n \leq \frac{\pi}{2} \quad (14)$$

Using Equation (13), the magnitude of the odd harmonics is given by the following:

$$b_n = \frac{4V_{dc}}{n\pi} [\cos(n\theta_1) + \cos(n\theta_2) + \dots + \cos(n\theta_s)] \quad (15)$$

Equation (16) shows the THD according to the IEEE 519 standard [40]; this equation is the property to optimize (minimize) and is called the objective function, while the switching angles calculation determines the output voltage quality.

$$THD(\%) = \left[\left(\frac{1}{V_1^2} \right) \sum_{n=3}^{\infty} \cos^2(V_n^2) \right]^{\frac{1}{2}} * 100 \quad (16)$$

where

$$V_n = \frac{4V_{dc}}{n\pi} \cos(n\theta_1) + \frac{4V_{dc}}{n\pi} \cos(n\theta_2) + \dots + \frac{4V_{dc}}{n\pi} \cos(n\theta_s) \quad (17)$$

Once the Equation (16) was defined as the objective function, the MFO algorithm was implemented by using a script in the MATLAB Software, and the algorithm was implemented under the following considerations:

- Number of particles: 30.
- Maximum number of iterations: 100.
- Logarithm spiral constant: 1.

The lb and the ub limits were defined according to Equation (14), where $lb = 0$ and $ub = \frac{\pi}{2}$ for the five- and seven-level CHBMLI. To test how fast the switching angles were obtained, the algorithm was tested up to 100 iterations.

The characteristics of the computer where the algorithm was implemented are as follows:

- Dell Precision 7530.
- Intel(R) Core(TM) i7-8850H CPU @ 2.60GHz.
- 32 GB of RAM DDR4.

3. Results

This section shows the obtained angle configurations for the five- and seven-level CHBMLI, offering a detailed account of their practical implementation within a dedicated laboratory prototype setup.

3.1. MFO Results

The resulting angles and their theoretical THD are shown in Table 1.

Table 1. Angles obtained using the MFO algorithm.

Angle	Five-Level CHBMLI	Seven-Level CHBMLI
θ_1	13.40°	8.69°
θ_2	41.91°	27.89°
θ_3	-	49.81°
%THD	15.29%	10.43%

As previously mentioned, the MFO algorithm underwent a series of iterations totaling up to 100. These iterations were performed to optimize the objective function outlined in Equations (16) and (17). Remarkably, in the context of the five-level CHBMLI configuration, it was found that a mere ten iterations sufficed to attain and sustain a commendable THD level of 15.29%, as demonstrated in Figure 5.

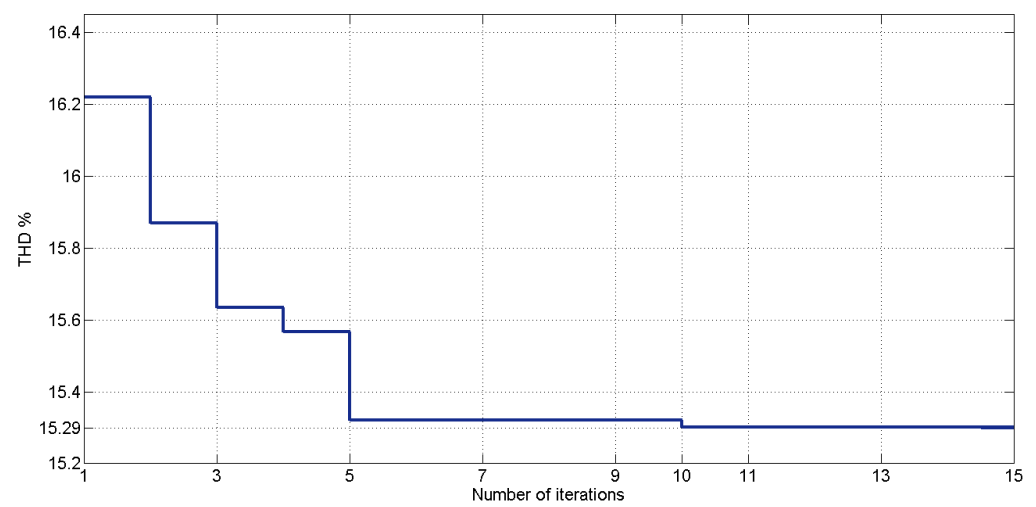


Figure 5. THD vs. iterations for the five-level CHBMLI.

Meanwhile, the algorithm exhibited impressive performance when dealing with the more complex seven-level CHBMLI configuration. It reached and maintained a remarkably low THD of 10.43% at the 33rd iteration, showcasing its efficiency and effectiveness, as shown in Figure 6.

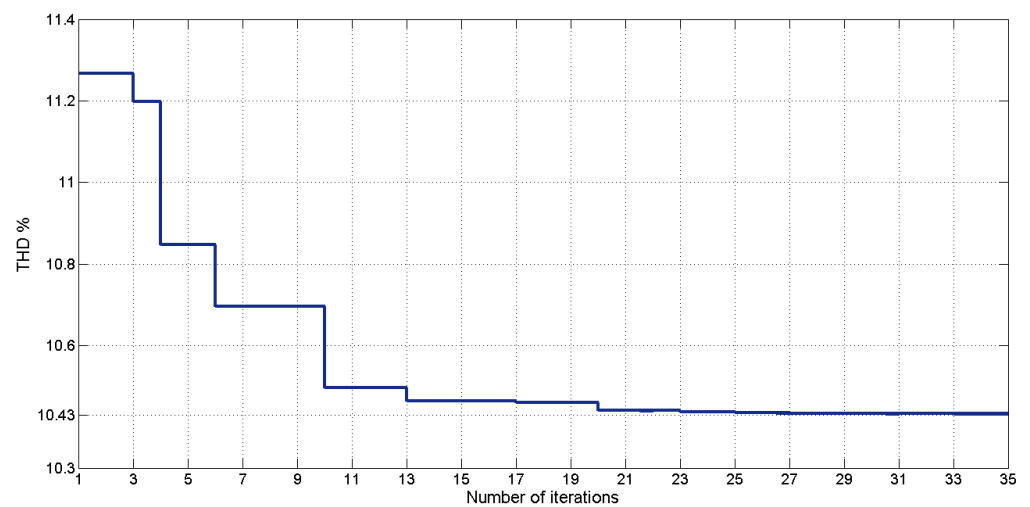


Figure 6. THD vs. iterations for the seven-level CHBMLI.

With the angles obtained in Table 1, the harmonic spectrum that should theoretically be obtained in the output voltage of the CHBMLI was calculated in Matlab, both for the five- and seven-level (Figures 7 and 8). This calculation was performed by graphing the sum values of Equation (16) and adding the value of the fundamental.

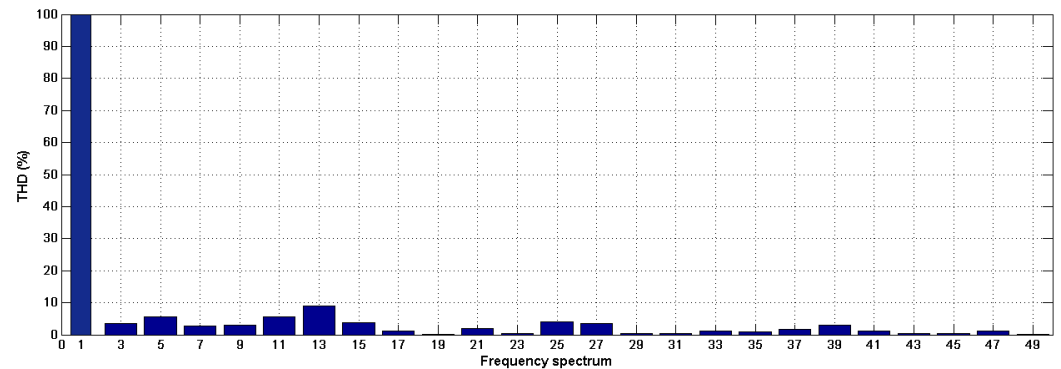


Figure 7. Five-level CHBMLI harmonic spectrum in Matlab.

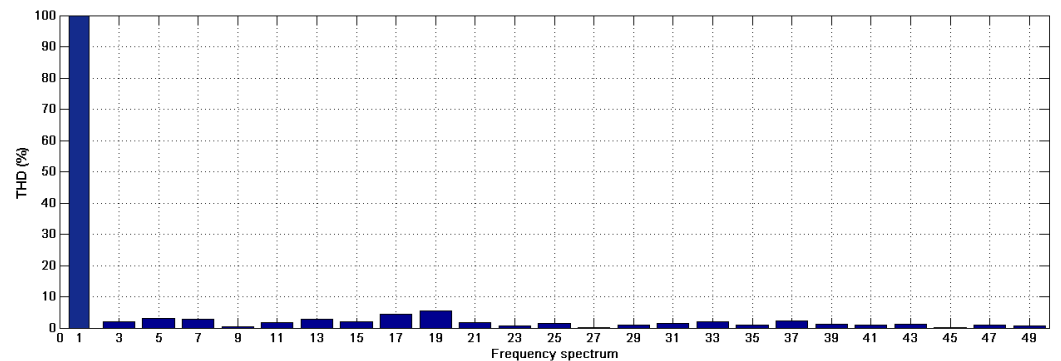


Figure 8. Seven-level CHBMLI harmonic spectrum in Matlab.

3.2. Implementation Results

As previously elucidated, the chosen topology for this particular endeavor was the five- and seven-level CHBMLI, with a resistive load at the output stage. The designed module is shown in Figure 9, where every nuanced detail of the inverter's configuration is presented. It is essential to underscore that the realization of this inverter's seven-level output configuration necessitated the judicious replication of the module mentioned above three times. The inverter features the STGW20NC60VD Insulated Gate Bipolar Transistors (IGBTs) as the switching semiconductor. The switching angles were implemented in the microcontroller PIC16F877A; this option has various advantages, such as low implementation cost and ease of program.

On the other hand, Figure 10 presents a detailed depiction of the prototype setup engineered to facilitate the generation of seven distinct voltage levels. This setup serves as a flexible platform capable of accommodating various level requirements, exemplified by the process of module removal, which is employed to tailor the output voltage waveform precisely to the desired configuration. The modular nature of this setup allows for adaptability, ensuring that the synthesis process can be seamlessly adjusted to attain specific voltage levels as necessitated by the application. Furthermore, within the context of this comprehensive exposition, it becomes evident that the visual representation encapsulated in Figure 8 not only conveys the structural intricacies of the prototype setup for the five and seven-level synthesis but also provides a discerning glimpse into the instrumental arsenal meticulously harnessed to scrutinize, monitor, and evaluate the characteristics of the output voltage waveform.

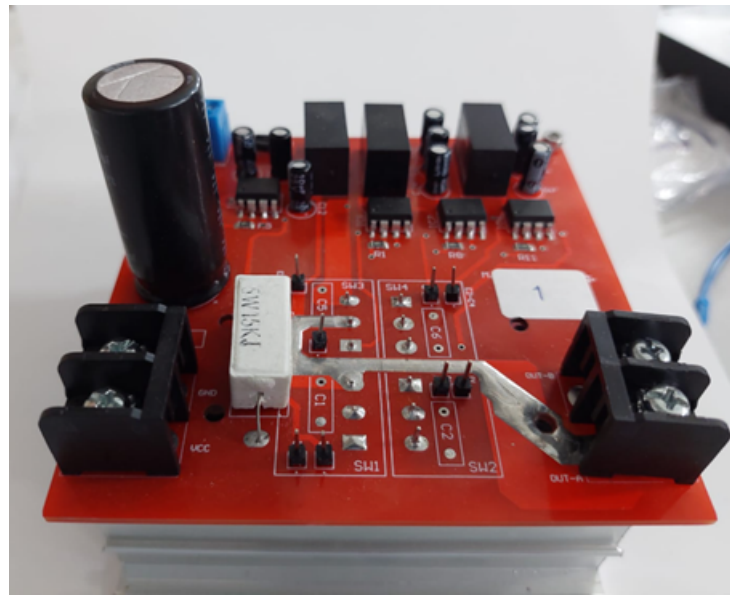


Figure 9. CHBMLI module.

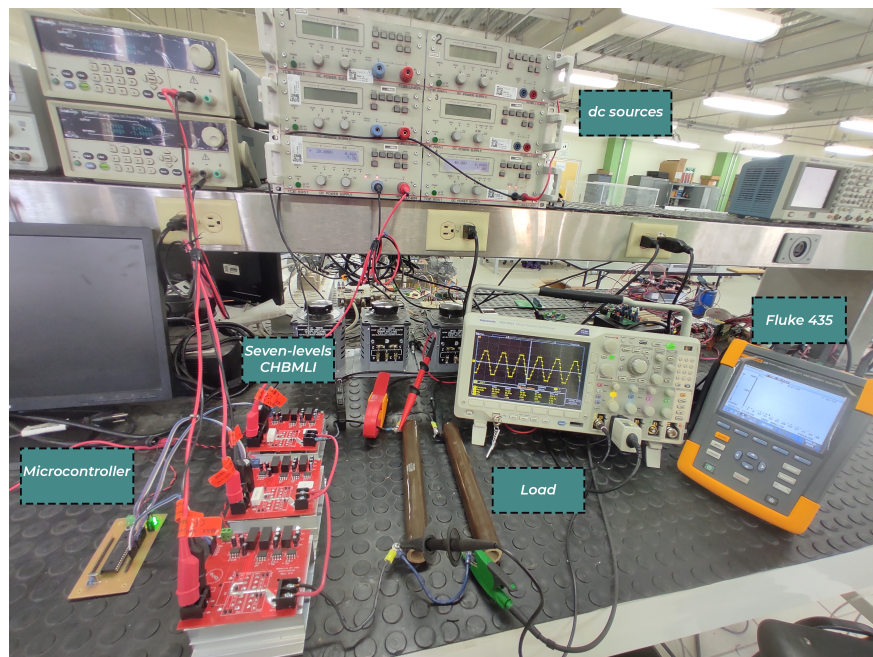


Figure 10. Seven-level CHBMLI prototype.

Table 2 provides an overview of the key parameters employed in the cascaded multilevel inverter configurations for both the five-level and seven-level setups.

Table 2. Main five- and seven-level CHBMLI parameters.

Parameters	Values
Voltage sources (five-level CHBMLI)	90 V each inverter
Voltage sources (seven-level CHBMLI)	60 V each inverter
Peak voltage	180 V
Load	R = 250 Ω, R = 100 Ω and R = 100 Ω with an AC motor detailed below
Frequency	60 Hz
Power	122.5 W

3.2.1. Five-Level CHBMLI Results

Figure 11 serves as an illuminating visual representation of the output voltage waveform with a resistive load of 250Ω , providing a detailed insight into the results of the synthesis process designed to achieve the desired five-level configuration; this waveform was obtained using a Tektroniks oscilloscope MDO3024. In this graphical depiction, these five levels' distinct and deliberate synthesis becomes readily apparent, showcasing a waveform characterized by its multi-level structure. Moreover, this waveform analysis affirms the successful attainment of specific operational objectives, as evidenced by the realization of a peak voltage precisely at the targeted magnitude of 180 V, harmonizing seamlessly with the intended specifications shown in Table 2. Additionally, the waveform's frequency is observed to align closely with the desired 60 Hz frequency, thereby confirming the meticulous precision and accuracy of the synthesis process.

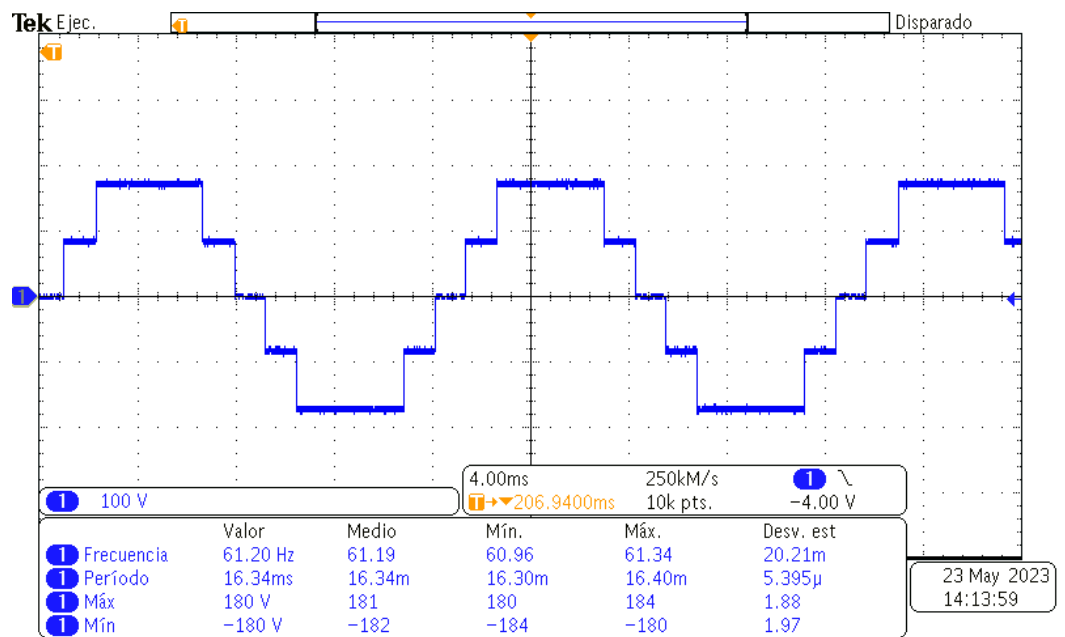


Figure 11. Five-level CHBMLI output voltage with $R = 250 \Omega$.

Figure 12 shows the output current waveform of the CHBMLI, which was also obtained using a Tektroniks oscilloscope MDO3024. Because the load of the five-level CHBMLI is resistive, the output voltage and the output current have the same form, and both signals are in phase.

The THD value of the voltage waveform was measured using the Power Quality Analyzer Fluke 435. The results of this THD measurement and the comprehensive Fast Fourier Transform (FFT) analysis, spanning up to the 49th harmonic, are visually represented in Figure 13 for reference and analysis. Notably, the THD value has been quantified at 15.3% in this specific instance.

As previously articulated, it is worth emphasizing that the OMTHD method diverges significantly from the SHE method in its primary objective. Unlike the SHE method, which is primarily focused on the eradication of low-order harmonics, the OMTHD approach prioritizes the reduction of the THD, thus addressing higher-order harmonics and overall waveform quality enhancement as opposed to exclusively targeting low-order harmonics elimination.

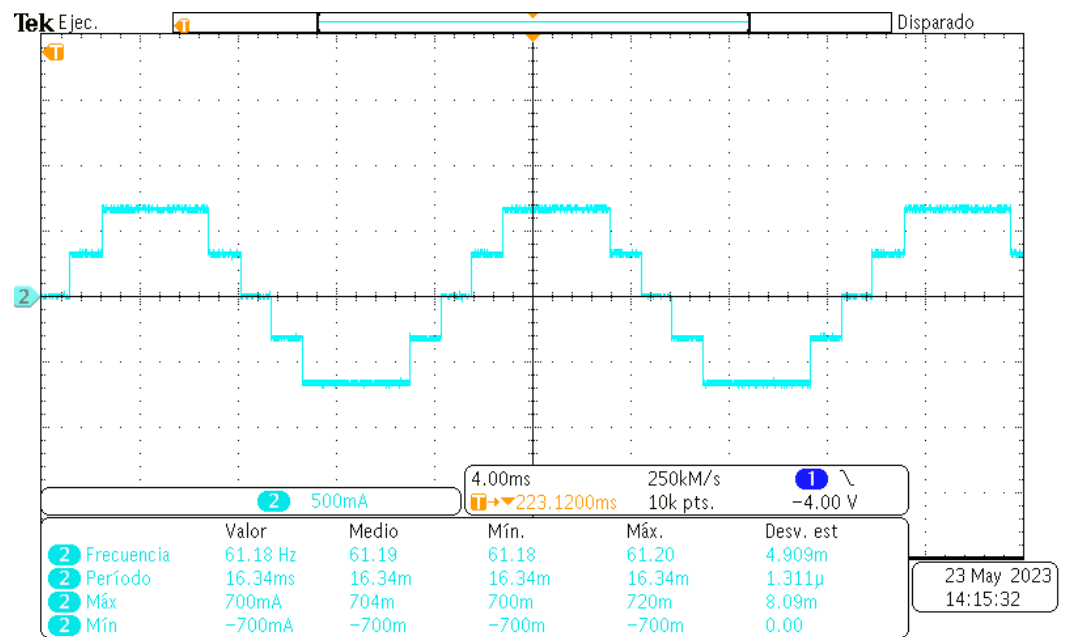


Figure 12. Five-level CHBMLI output voltage with $R = 250 \Omega$.

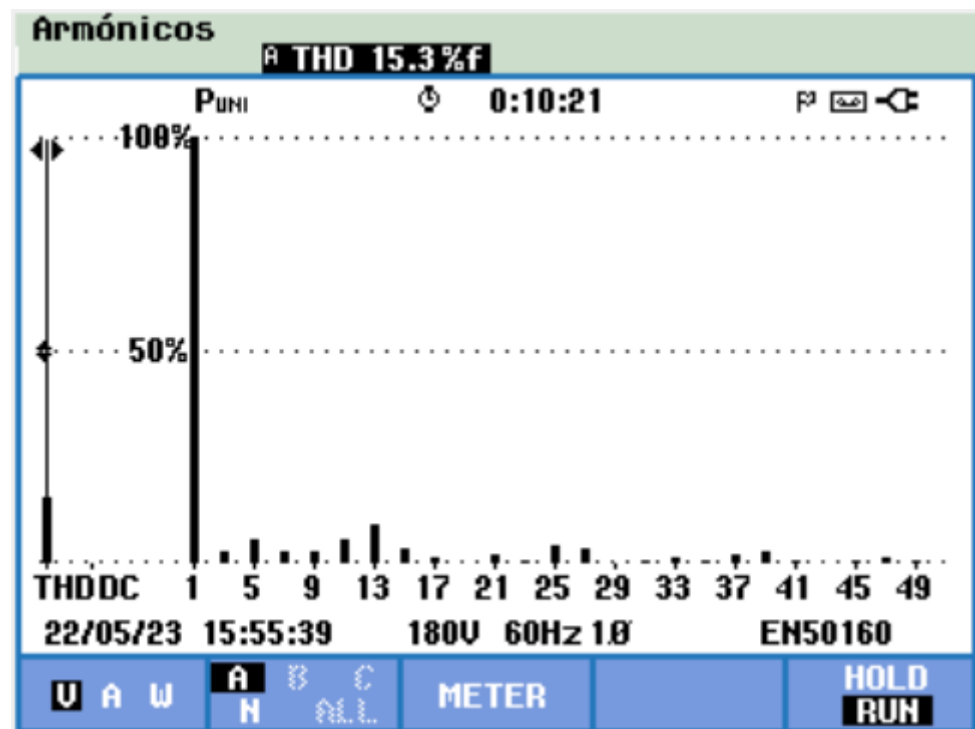


Figure 13. Fast Fourier Transform of the five-level CHBMLI output voltage with $R = 250 \Omega$.

Subsequently, a 100Ω resistive load was connected to the output of the CHBMLI. The output voltage is shown in Figure 14, while the output current is shown in Figure 15. As with the previous load, the five levels of the output voltage can be seen, and the current has the same shape as the voltage.

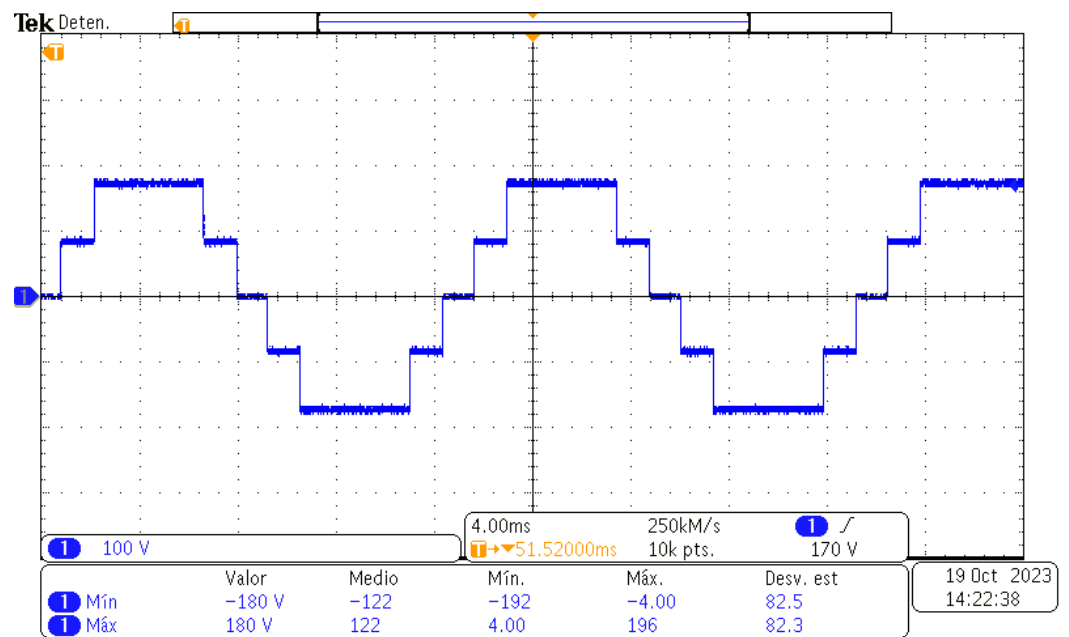


Figure 14. Five-level CHBMLI output voltage with $R = 100 \Omega$.

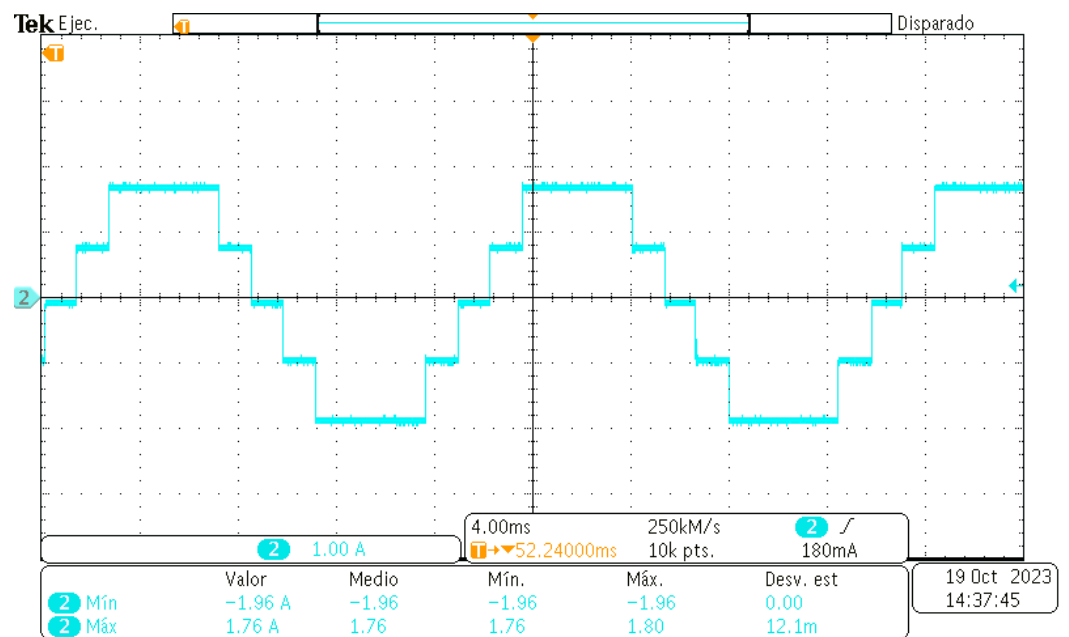


Figure 15. Five-level CHBMLI output voltage with $R = 100 \Omega$.

Figure 16 shows the THD value of the voltage waveform; it can be observed that a THD value of 15.3% was obtained just like with the resistive load of 250 Ω .

The last load connected to the five-level CHBMLI was an RL load. The load consists of a 100 Ω resistor and an brushless AC motor with the following characteristics:

- Power: 1/20 HP;
- Current: 2.0 A;
- Voltage: 127 Vrms;
- Frequency: 60 Hz;
- Speed: 1550 RPM.

This AC motor is shown in Figure 17.

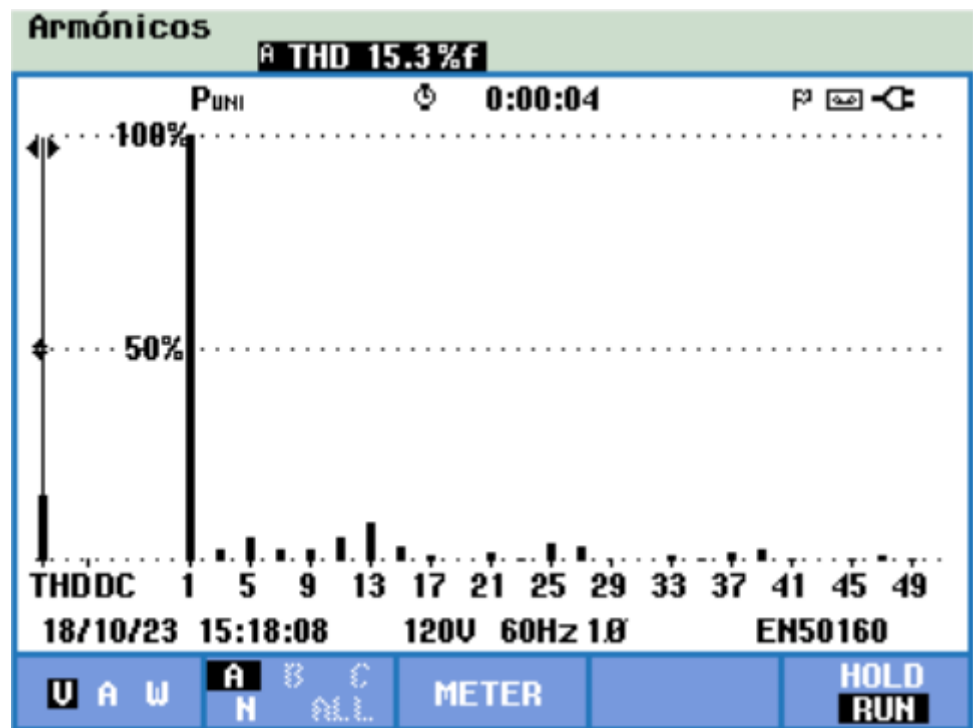


Figure 16. Fast Fourier Transform of the five-level CHBMLI output voltage with $R = 100 \Omega$.



Figure 17. Five-level CHBMLI output voltage with the RL load.

Figure 18 shows the output voltage with the RL load, while Figure 19 shows the output current. Because the load now has an inductive component, the output current waveform is no longer the same as the output voltage waveform.

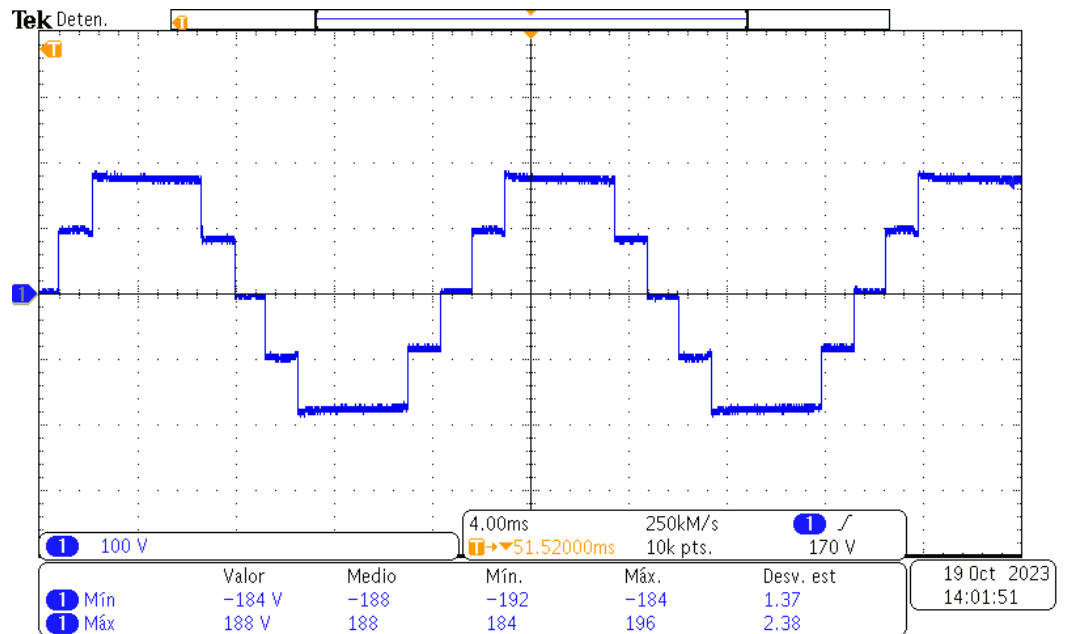


Figure 18. Five-level CHBMLI output voltage with the RL load.

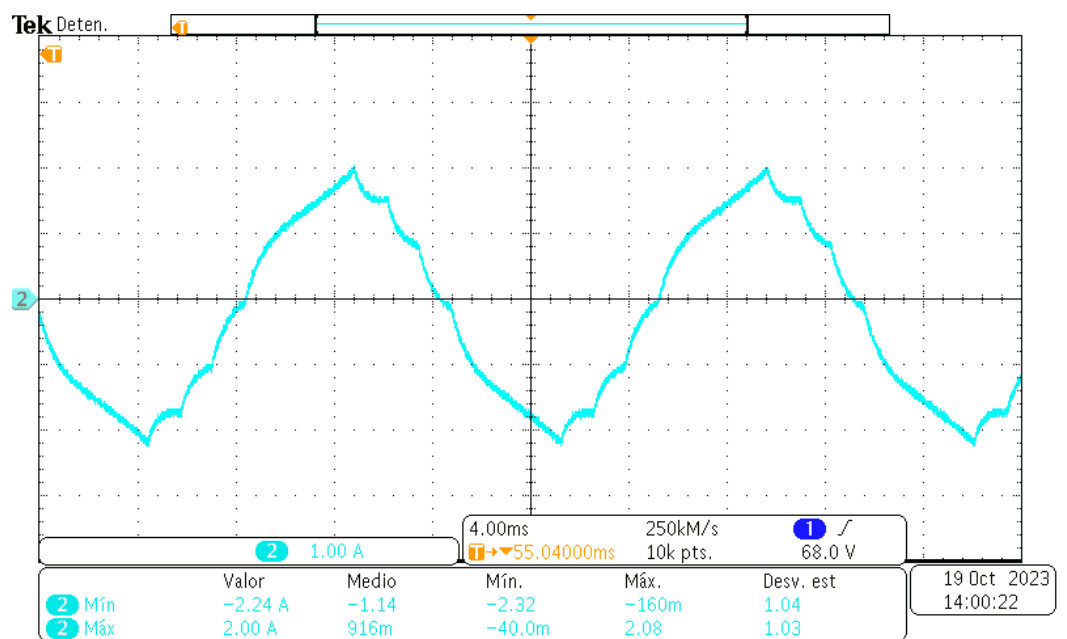


Figure 19. Five-level CHBMLI output current with the RL load.

It can be seen that, even with an inductive load, the voltage maintains its shape, and the value of the output THD does not change, as seen in Figure 20, where the THD remains with a value of 15.3%.

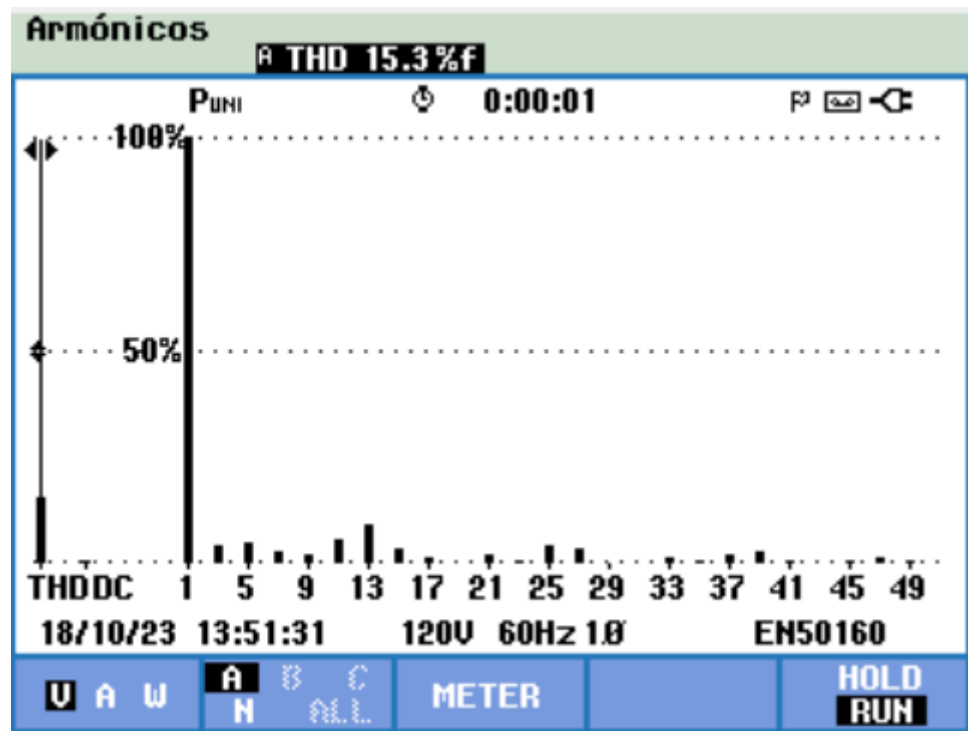


Figure 20. Fast Fourier Transform of the five-level CHBMLI output voltage with the RL load.

3.2.2. Seven-Level CHBMLI Results

Concerning the outcomes derived from the seven-level experimental configuration, an illustrative representation of the output voltage waveform is comprehensively displayed in Figure 21 and with a resistive load of $R = 250 \Omega$, offering a vivid depiction of the distinctive characteristics inherent to the seven-level CHBMLI. As we observe this graphical representation, we can discern that, akin to the findings obtained from the five-level CHBMLI analysis, the output voltage waveform exhibits remarkable symmetry, and its frequency closely aligns with the nominal 60 Hz standard. It can also be observed that the peak voltage in this configuration reaches a magnitude of 180 V. Meanwhile, Figure 22 shows the current waveform with the resistive load of $R = 250 \Omega$.

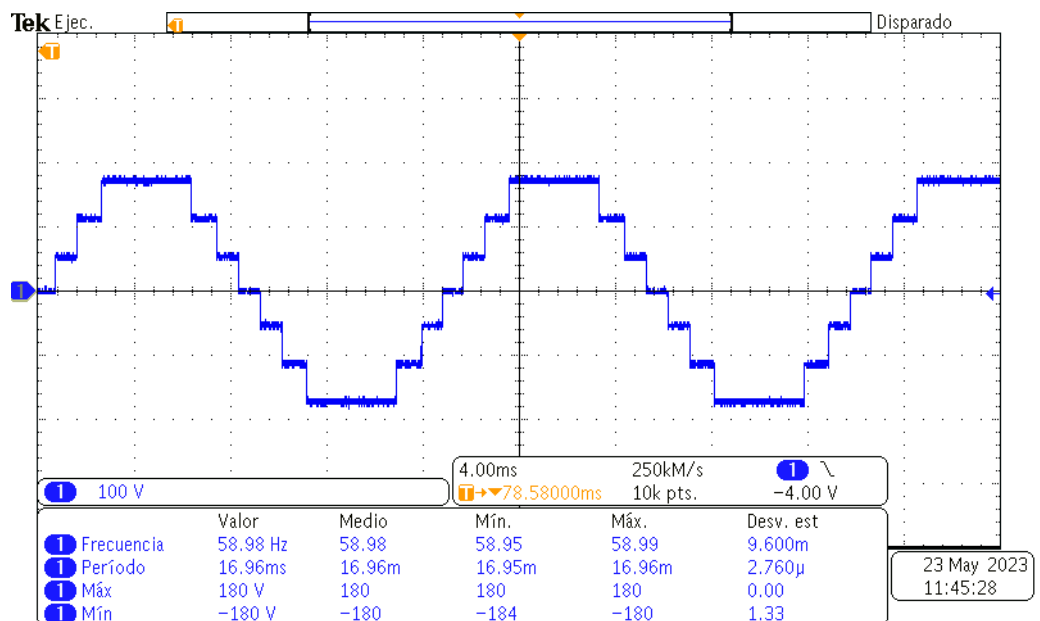


Figure 21. Seven-level CHBMLI output voltage with $R = 250 \Omega$.

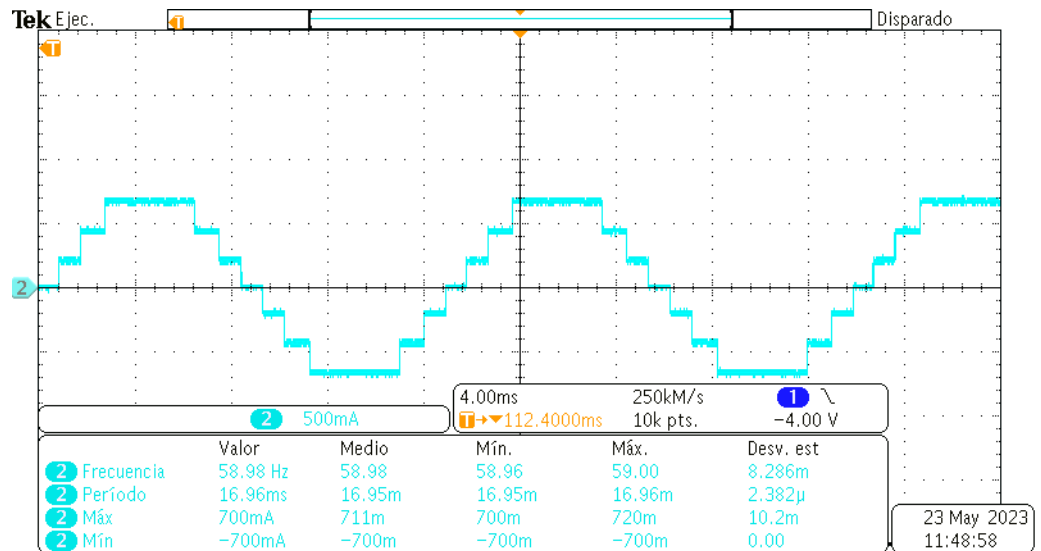


Figure 22. Seven-level CHBMLI output current with $R = 250 \Omega$.

Similar to the findings observed in the five-level configuration, a comprehensive assessment of the THD was conducted in the seven-level setup using the sophisticated Power Quality Analyzer Fluke 435. Notably, in this specific instance, the THD measurement yielded a value of 10.5%, which is visually presented and elaborated upon in Figure 23. It is worth highlighting that, upon closer examination, it becomes evident that the third harmonic component exhibited a somewhat sporadic reduction in this particular case. However, as previously elucidated, it is essential to emphasize that the OMTHD method’s primary objective is not explicitly geared toward eliminating or systematically reducing low-order harmonics. But, rather, its principal focus resides in the overarching goal of mitigating and diminishing the THD across the entire spectrum of harmonics, thus enhancing the overall quality and fidelity of the electrical waveform under analysis. This nuanced distinction underscores the multifaceted nature and strategic intent of the OMTHD methodology.

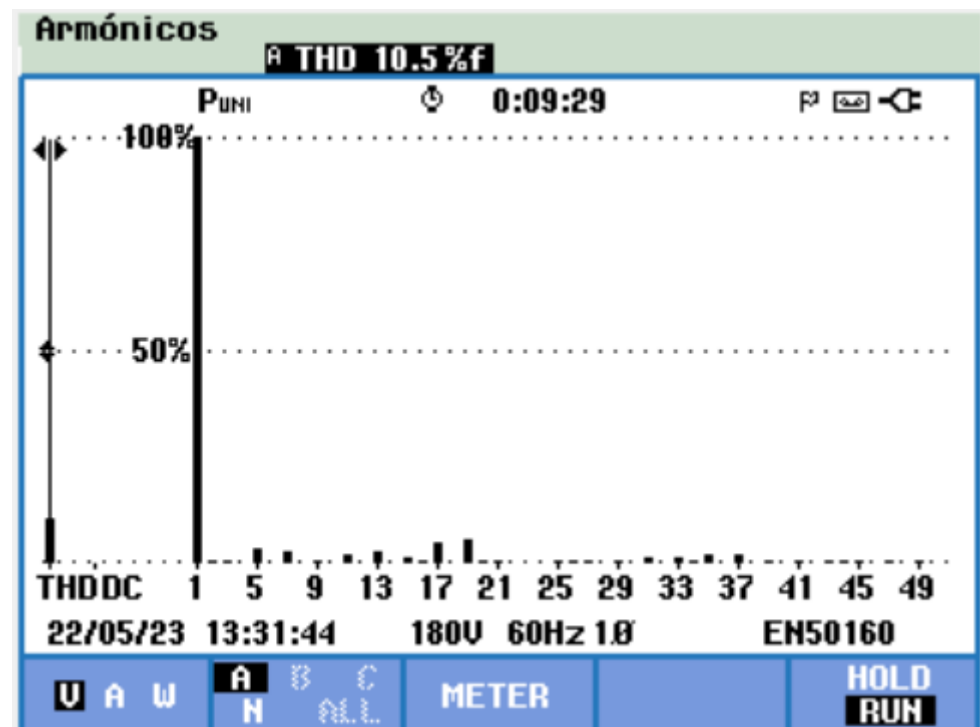


Figure 23. Fast Fourier Transform of the seven-level CHBMLI output voltage with $R = 250 \Omega$.

Then, a 100 Ω resistive load was connected to the CHBMLI. Figure 24 shows the output voltage; the output current can be observed in Figure 25. The output voltage waveform keeps the same shape as the 250 Ω resistive load.

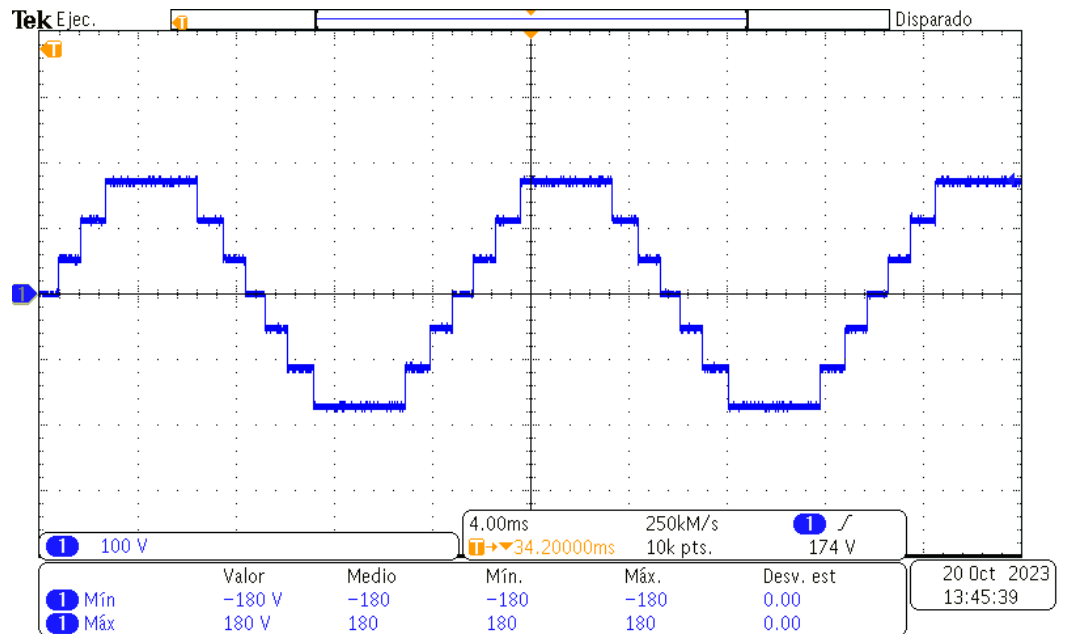


Figure 24. Seven-level CHBMLI output voltage with R = 100 Ω.

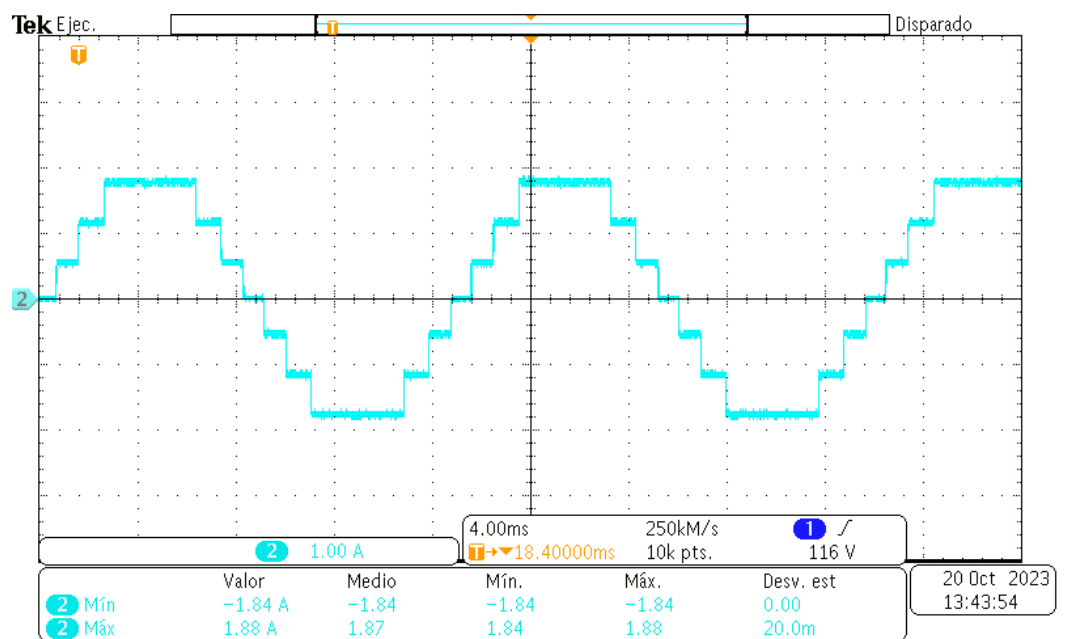


Figure 25. Seven-level CHBMLI output current with R = 100 Ω.

Figure 26 shows the THD with the resistive load of 100 Ω; it can be seen that this value, as well as the harmonic spectrum, is the same as the one shown in Figure 23.

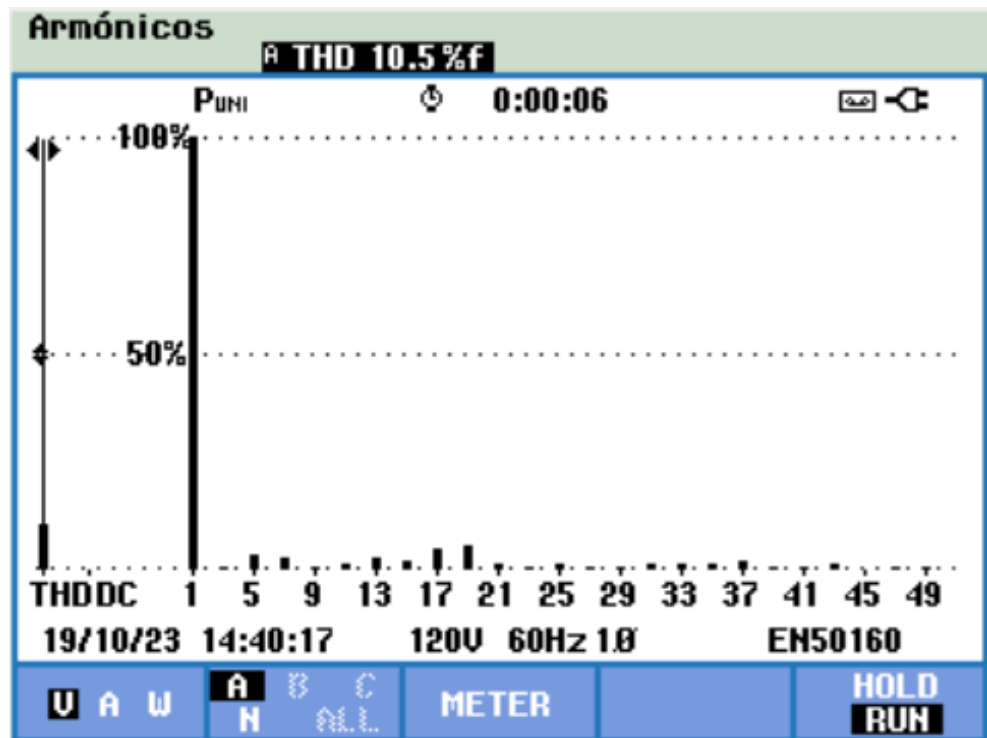


Figure 26. Fast Fourier Transform of the seven-level CHBMLI output voltage with $R = 100 \Omega$.

As with the five-level CHBMLI, an RL load consisting of a 100Ω resistor and a brushless AC motor was also connected. The characteristics of the motor have already been previously stated. Figure 27 shows the output voltage waveform, while Figure 28 shows the current waveform. Because this is an RL load, the current waveform differs from the voltage waveform.

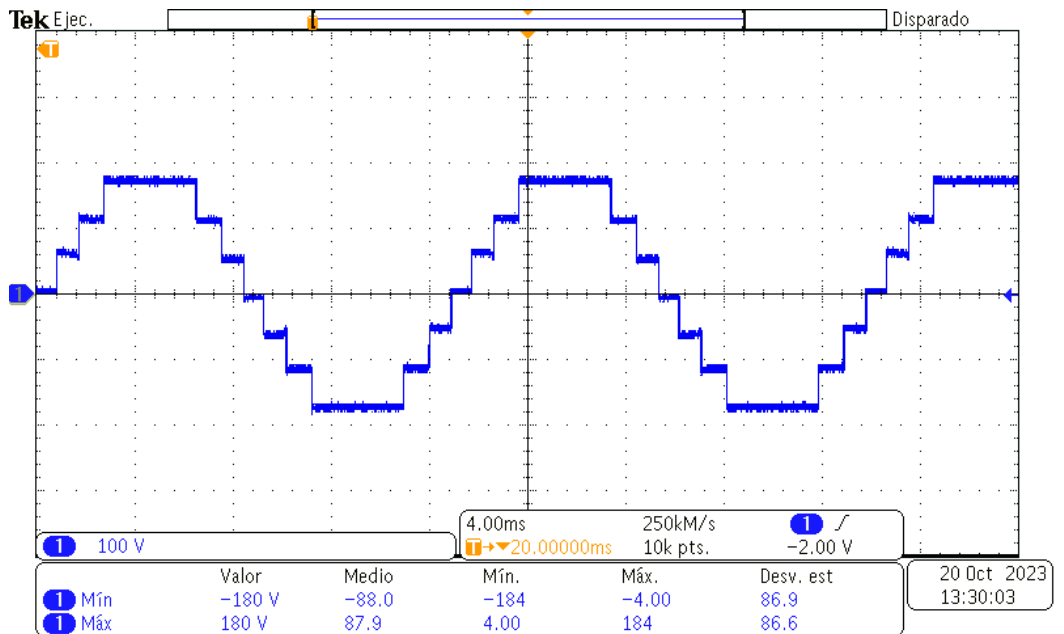


Figure 27. Seven-level CHBMLI output voltage with $R = 100 \Omega$.

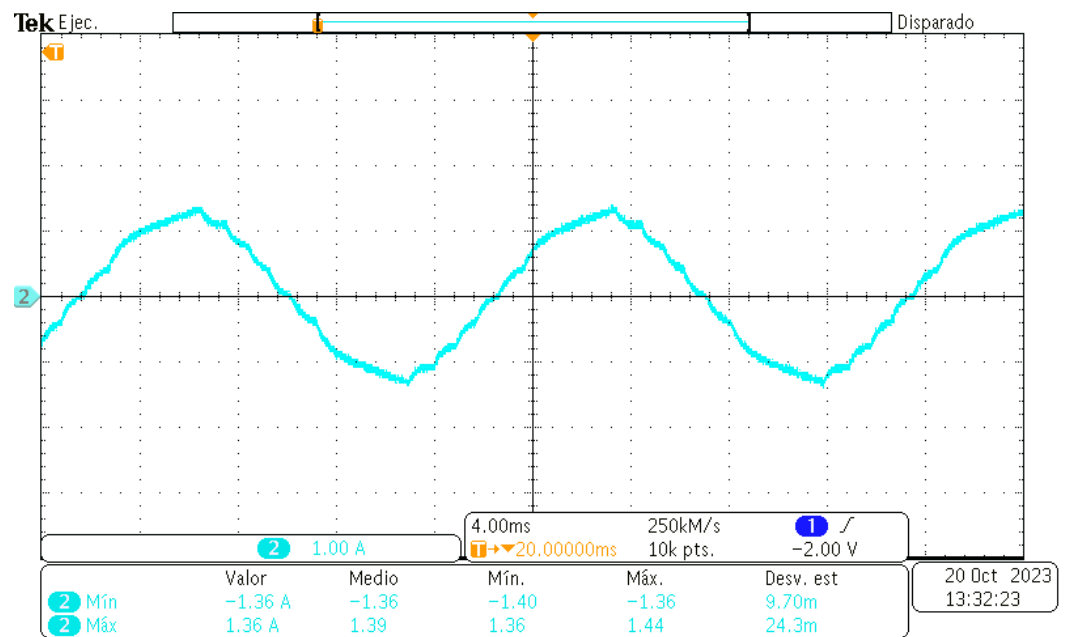


Figure 28. Seven-level CHBMLI output current with $R = 100 \Omega$.

Regarding the THD value for the RL load, the obtained value of 10.5% can be observed in Figure 29.

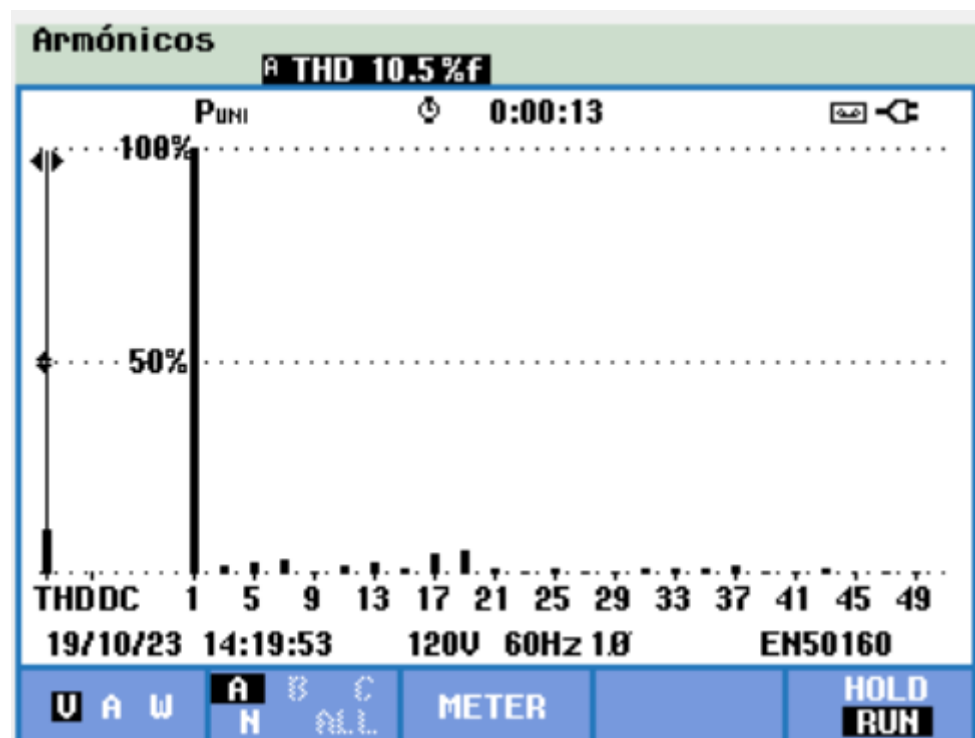


Figure 29. Fast Fourier Transform of the seven-level CHBMLI output voltage with the RL load.

4. Discussion

The experimental results obtained in a laboratory prototype were similar to the theoretical results in both cases (Table 3), which means that the implementation of the switching angles in the microcontroller was correct. It can be seen that the THD was consistent in the output voltage waveform with all the tested loads as expected.

Table 3. Comparison of the obtained theoretical and experimental THD.

Levels in the CHBMLI	Theoretical % THD	Experimental % THD
Five	15.29%	15.3%
Seven	10.43%	10.5%

These outcomes were juxtaposed with findings documented in the literature in order to assess the effectiveness of applying the MFO algorithm. This comparison includes both metaheuristic and non-metaheuristic methods, as well as simulation and experimental results; the comparison for the five-level CHBMLI is shown in Table 4, while the comparison for the seven-level CHBMLI is shown in Table 5.

Table 4. Comparison of the literature for the five-level CHBMLI.

Paper	Algorithm	Angle Values	THD
[13]	ABC	$\theta_1 = 13.408^\circ$ $\theta_2 = 41.915^\circ$	15.3% (Experimental)
[13]	Matlab fsolve function	$\theta_1 = 12.00^\circ$ $\theta_2 = 48.00^\circ$	16.2% (Experimental)
[14]	PSO	$\theta_1 = 13.34^\circ$ $\theta_2 = 41.79^\circ$	15.2% (Experimental)
[15]	NR	$\theta_1 = 19.00^\circ$ $\theta_2 = 43.00^\circ$	17.23% (Simulation)
[15]	GA	$\theta_1 = 17.02^\circ$ $\theta_2 = 43.01^\circ$	16.14% (Simulation)
[11]	NR	$\theta_1 = 11.80^\circ$ $\theta_2 = 41.77^\circ$	15.51% (Simulation)
[11]	GA	$\theta_1 = 14.33^\circ$ $\theta_2 = 42.10^\circ$	15.35% (Simulation)
[11]	PSO	$\theta_1 = 13.40^\circ$ $\theta_2 = 41.91^\circ$	15.29% (Simulation)
This paper	MFO	$\theta_1 = 13.40^\circ$ $\theta_2 = 41.91^\circ$	15.3% (Experimental)

In Table 4, compared with the five levels of the CHBMLI, the MFO algorithm obtained a better THD (lower THD value) in five of the eight reported cases, and the same THD was obtained in one case. The authors of references [11,13] report a lower THD compared to the MFO algorithm implemented in this paper, and, interestingly, the MFO switching angles were the same as those reported in reference [11] with the PSO algorithm. However, the results reported in references [11,13] were obtained through simulation, whereas this paper presents experimental results, where the inverter's real semiconductors and the microcontroller's processing time play an important part. Regarding the harmonic spectrum of references [11,13], the authors consider up to the 49th harmonic, the same harmonic spectrum considered in this paper.

The results shown in reference [15] consider up to the 49th harmonic, as in this paper, but in reference [15], the authors only present simulation results.

Performing a more exhaustive comparison of this proposal with the presentation in reference [14] shows that both proposals were carried out experimentally with the same objective function. Similarly, the voltage waveform was implemented with a microcontroller, although in reference [14], a PIC16F628A microcontroller was used, while in this paper, the PIC16F877A microcontroller was used. This article and reference [14] considered the harmonic spectrum up to the 49th harmonic. The same power quality analyzer (Fluke 435) is used in both papers. Due to the above, although reference [14] shows a better result, the

difference percentage is insignificant, so this paper's proposal can obtain as good results as one of the most used algorithms with this objective function.

Table 5. Comparison of the literature for the seven-level CHBMLI.

Paper	Algorithm	Angle Values	THD
[15]	NR	$\theta_1 = 13.06^\circ$ $\theta_2 = 26.00^\circ$ $\theta_3 = 57.00^\circ$	12.49% (Simulation)
[15]	GA	$\theta_1 = 12.00^\circ$ $\theta_2 = 26.93^\circ$ $\theta_3 = 55.49^\circ$	11.57% (Simulation)
[11]	NR	$\theta_1 = 8.00^\circ$ $\theta_2 = 30.00^\circ$ $\theta_3 = 56.00^\circ$	11.09% (Simulation)
[11]	GA	$\theta_1 = 8.08^\circ$ $\theta_2 = 28.35^\circ$ $\theta_3 = 50.18^\circ$	10.47% (Simulation)
[11]	PSO	$\theta_1 = 8.69^\circ$ $\theta_2 = 27.89^\circ$ $\theta_3 = 49.81^\circ$	10.42% (Simulation)
This paper	MFO	$\theta_1 = 8.69^\circ$ $\theta_2 = 27.89^\circ$ $\theta_3 = 49.81^\circ$	10.5% (Experimental)

Regarding the seven levels of the CHBMLI, Table 5 shows that the MFO algorithm obtained a better THD (lower THD value) in four of the six reported cases. Regarding the results reported in reference [11] with the PSO algorithm, the same objective function is used in this paper, and the same harmonic spectrum considers the harmonics up to the 49th. Because reference [11] shows simulation results, comparing the microcontroller or the power quality analyzer is impossible. The THD obtained in reference [11] is lower than the THD obtained in this paper; however, reference [11] only shows simulation results with ideal semiconductors of the inverter. As with the five-level CHBMLI comparisons, in reference [15], the authors consider the same harmonic spectrum used in this paper, but only simulation results are shown.

5. Conclusions

This study utilizes the Moth–Flame Optimization algorithm to minimize Total Harmonic Distortion in a CHBMLI topology. The algorithm was applied to five- and seven-level CHBMLI topologies, resulting in optimized switching angles. These angles were implemented on a laboratory prototype, achieving both levels' experimental THD values. The experimental THD values were compared against the theoretical ones, leading to a maximum difference of 0.07%.

Furthermore, the optimized switching angles and the experimental THD values were compared with those reported in the available literature obtained using different optimization methods. The results indicated that, for the five-level inverter, the THD obtained using the MFO algorithm is superior to that reported in most of the literature, with a percentage difference of up to 1.93%. However, as reported in the literature, the PSO algorithm achieves a better THD value but with a maximum percentage difference of only 0.1%. In the case of the seven-level inverter results, the MFO algorithm demonstrates a superior THD value, exhibiting a maximum percentage difference of 1.9% compared to most optimization algorithms used in the existing literature. Again, the PSO algorithm yields a better THD value; however, the difference from the MFO algorithm is only 0.8%. It is important to remark that most of the THD values reported in the literature were obtained through simu-

lation, while the THD obtained in this paper were through a laboratory prototype, where the components of the inverter change the obtained THD in the output voltage waveform.

The MFO algorithm can be used in CHBMLI of higher levels, and the relatively limited application of this algorithm in power converters may open opportunities for its use in designing isolated Direct Current to Direct Current converters; this could consider cost, volume, heat sink weight, and thermal resistance. Additionally, it is worth mentioning the relatively few iterations required to achieve reliable results, unlike other optimization methods. Regarding the control tuning of the inverter controllers, the tuning parameters are another optimization problem that can be explored with the MFO algorithm.

Author Contributions: Conceptualization, A.R.L. and O.A.L.-N.; methodology, M.G.M.-E. and C.A.T.-C.; software, O.A.L.-N.; validation, F.D.J.S.-V. and J.Y.R.-M.; formal analysis, G.O.-T. and R.P.-Z.; investigation, A.R.L. and M.A.L.-O.; resources, M.M.-G. and J.G.R.; writing—original draft preparation, A.R.L.; writing—review and editing, O.A.L.-N.; visualization, M.R.-M. and J.C.M.-S.; supervision, A.R.L. and F.D.J.S.-V. All authors have read and agreed to the published version of the manuscript.

Funding: This research received no external funding.

Institutional Review Board Statement: Not applicable.

Informed Consent Statement: Not applicable.

Data Availability Statement: Data is contained within the article.

Conflicts of Interest: The authors declare no conflict of interest.

Abbreviations

The following abbreviations are used in this manuscript:

THD	Total Harmonic Distortion
CHBMLI	Cascade H-Bridge Multilevel Inverter Topology
SHE	Selective Harmonic Elimination
OMTHD	Optimal Minimization of the Total Harmonic Distortion
GA	Genetic Algorithm
PSO	Particle Swarm Optimization
ABC	Artificial Bee Colony
NR	Newton Raphson
MFO	Moth–Flame Optimization
DC	Direct Current
IGBT	Insulated Gate Bipolar Transistor
FFT	Fast Fourier Transform
Vrms	Voltage in rms

References

- Hasan, N.S.; Rosmin, N.; Osman, D.A.A.; Musta'amal@Jamal, A.H. Reviews on multilevel converter and modulation techniques. *Renew. Sustain. Energy Rev.* **2017**, *80*, 163–174. [[CrossRef](#)]
- Barros, L.A.; Martins, A.P.; Pinto, J.G. A Comprehensive Review on Modular Multilevel Converters, Submodule Topologies, and Modulation Techniques. *Energies* **2022**, *15*, 1078. [[CrossRef](#)]
- Colak, I.; Kabalci, E.; Bayindir, R. Review of multilevel voltage source inverter topologies and control schemes. *Energy Convers. Manag.* **2011**, *52*, 1114–1128. [[CrossRef](#)]
- Malinowski, M.; Gopakumar, K.; Rodriguez, J.; Perez, M.A. A survey on cascaded multilevel inverters. *IEEE Trans. Ind. Electron.* **2010**, *57*, 2197–2206. [[CrossRef](#)]
- Ali Khan, M.Y.; Liu, H.; Yang, Z.; Yuan, X. A Comprehensive Review on Grid Connected Photovoltaic Inverters, Their Modulation Techniques, and Control Strategies. *Energies* **2020**, *13*, 4185. [[CrossRef](#)]
- Koshti, A.K.; Rao, M. A Brief review on multilevel inverter topologies. In Proceedings of the 2017 International Conference on Data Management, Analysis and Innovation (ICDMAI), Pune, India, 24–26 February 2017; pp. 187–193.
- Bertin, T.; Despesse, G.; Thomas, R. Comparison between a Cascaded H-Bridge and a Conventional H-Bridge for a 5-kW Grid-Tied Solar Inverter. *Electronics* **2023**, *12*, 1929. [[CrossRef](#)]

8. Jahan, H.K.; Kurdkandi, N.V.; Abapour, M.; Zare, K.; Hosseini, S.H.; Yang, Y.; Blaabjerg, F. Common-ground-type single-source high step-up cascaded multilevel inverter for transformerless PV applications. *Mathematics* **2020**, *8*, 1716. [[CrossRef](#)]
9. Shin, C.; Lim, K.; Petrus, S.D.; Choi, J. Harmonics compensation for grid-connected inverter caused by local nonlinear load. In Proceedings of the 2017 19th International Conference on Electrical Drives and Power Electronics (EDPE), Dubrovnik, Croatia, 4–6 October 2017; pp. 46–52. [[CrossRef](#)]
10. Lim, K.; Simatupang, D.P.; Choi, J. PR based output voltage regulation for harmonic compensation under islanded mode of microgrid with magnitude restoration. In Proceedings of the 2017 IEEE 3rd International Future Energy Electronics Conference and ECCE Asia (IFEEC 2017—ECCE Asia), Kaohsiung, Taiwan, 3–7 June 2017; pp. 1920–1925. [[CrossRef](#)]
11. Marín-Reyes, M.; Aguayo-Alquicira, J.; De León-Aldaco, S.E. Calculation of Optimal Switching Angles for a Multilevel Inverter Using NR, PSO, and GA- a Comparison. *Eur. J. Electr. Eng.* **2020**, *22*, 349–355. [[CrossRef](#)]
12. Ajami, A.; Oskuee, M.R.J.; Mokhberdorani, A.O. Implementation of novel technique for selective harmonic elimination in multilevel inverters based on ICA. *Adv. Power Electron.* **2013**, *2013*, 847365. [[CrossRef](#)]
13. Lopez, A.R.; Cortés, C.J.; Muñoz, C.A.; Alonso, L.A.; Muñoz Moreno, G.; Vazquez, G.; Sosa, J.M.; De Leon Aldaco, S.; Aguayo, J. Optimal Switching Angles Calculation for a Multilevel Inverter Through the ABC Algorithm. In Proceedings of the 2022 IEEE International Autumn Meeting on Power, Electronics and Computing (ROPEC 2022), Ixtapa, Mexico, 9–11 November 2022. [[CrossRef](#)]
14. Lopez, A.R.; Cortes, C.J.; Limones-Pozos, C.A.; Sosa, J.M.; Aguayo, J.; De Leon Aldaco, S. Optimal Switching Angles Calculation for a Multilevel Inverter through the SHE Method and the PSO Algorithm, a comparison. In Proceedings of the 2020 IEEE International Autumn Meeting on Power, Electronics and Computing (ROPEC 2020), Ixtapa, Mexico, 10–12 November 2020. [[CrossRef](#)]
15. Reyes, M.M.; Alquicira, J.A.; Aldaco, S.D.L.; Campos, E.M.A.; Severiano, Y.R. Calculation of Optimal Switching Angles for a Multilevel Inverter using NR and GA-a comparison. In Proceedings of the 14th IEEE International Conference on Power Electronics, Doha, Qatar, 10–12 April 2018; pp. 22–27.
16. Yousefpoor, N.; Fathi, S.H.; Farokhnia, N.; Abyaneh, H.A. THD Minimization Applied Directly on the Line-to-Line Voltage of Multilevel Inverters. *IEEE Trans. Ind. Electron.* **2012**, *59*, 373–380. [[CrossRef](#)]
17. De Leon-Aldaco, S.E.; Calleja, H.; Aguayo Alquicira, J. Metaheuristic Optimization Methods Applied to Power Converters: A Review. *IEEE Trans. Power Electron.* **2015**, *30*, 6791–6803. [[CrossRef](#)]
18. Alamri, B.; Darwish, M. Precise modelling of switching and conduction losses in cascaded h-bridge multilevel inverters. In Proceedings of the Universities Power Engineering Conference, Cluj-Napoca, Romania, 2–5 September 2014. [[CrossRef](#)]
19. Kumar, A.; Dasgupta, A.; Chatterjee, D. Harmonic mitigation of cascaded multilevel inverter using particle swarm optimization technique. In Proceedings of the IEEE International Conference on Power Electronics, Drives and Energy Systems (PEDES 2016), Trivandrum, India, 14–17 December 2016; pp. 1–6. [[CrossRef](#)]
20. Chatterjee, A.; Rastogi, A.; Rastogi, R.; Saini, A.; Sahoo, S.K. Selective Harmonic Elimination of Cascaded H-Bridge Multilevel Inverter using Genetic Algorithm. In Proceedings of the International Conference on Innovations in Power and Advance Computing Technologies (i-PACT2017), Vellore, India, 21–22 April 2017; pp. 1–4.
21. Sahoo, S.K.; Saha, A.K.; Ezugwu, A.E.; Agushaka, J.O.; Abuhaija, B.; Alsoud, A.R.; Abualigah, L. *Moth Flame Optimization: Theory, Modifications, Hybridizations, and Applications*; Springer: Dordrecht, The Netherlands, 2023; Volume 30, pp. 391–426. [[CrossRef](#)]
22. Mirjalili, S. Moth-flame optimization algorithm: A novel nature-inspired heuristic paradigm. *Knowl.-Based Syst.* **2015**, *89*, 228–249. [[CrossRef](#)]
23. Nadimi-Shahraki, M.H.; Zamani, H.; Fatahi, A.; Mirjalili, S. MFO-SFR: An Enhanced Moth-Flame Optimization Algorithm Using an Effective Stagnation Finding and Replacing Strategy. *Mathematics* **2023**, *11*, 862. [[CrossRef](#)]
24. Rezk, H.; Zaky, M.M.; Alhaider, M.; Tolba, M.A. Robust Fractional MPPT-Based Moth-Flame Optimization Algorithm for Thermoelectric Generation Applications. *Energies* **2022**, *15*, 8836. [[CrossRef](#)]
25. Shaikh, M.S.; Raj, S.; Ikram, M.; Khan, W. Parameters estimation of AC transmission line by an improved moth flame optimization method. *J. Electr. Syst. Inf. Technol.* **2022**, *9*. [[CrossRef](#)]
26. Hussien, S.A.; Deab, M.A.; Alrowais, F. Maximization of the power delivered from permanent magnet synchronous generator wind energy conversion system to the grid based on using moth flame optimization. *Indones. J. Electr. Eng. Comput. Sci.* **2022**, *27*, 1347–1357. [[CrossRef](#)]
27. Nadimi-shahraki, M.H.; Fatahi, A.; Zamani, H.; Mirjalili, S.; Oliva, D. Hybridizing of Whale and Moth-Flame Optimization Algorithms to Solve Diverse Scales of Optimal Power Flow Problem. *Electronics* **2022**, *11*, 831. [[CrossRef](#)]
28. Saravanan, L.; Sozhamannan, G.S.; Velmurugan, K.; Venkatachalnpathy, V.S. MFO-optimized constitutive model for a hybrid aluminum nanocomposite. *Mater. Today Proc.* **2021**, *44*, 2366–2372. [[CrossRef](#)]
29. Cuevas, E.; Fausto, F.; Gálvez, J.; Rodríguez, A. *MATLAB Computación Metaheurística y Bio-Inspirada*, 1st ed.; Alfaomega Grupo, Ed.; MATLAB: Natick, MA, USA, 2022; p. 420.
30. Ceylan, O. Harmonic elimination of multilevel inverters by moth-flame optimization algorithm. In Proceedings of the 2016 International Symposium on Industrial Electronics (INDEL 2016—Proceedings), Banja Luka, Bosnia and Herzegovina, 3–5 November 2016. [[CrossRef](#)]
31. Danin, Z.; Sharma, A.; Averbukh, M.; Arabinda, M. Improved Moth Flame Optimization Approach for Parameter Estimation of Induction Motor. *Energies* **2022**, *15*, 8834. [[CrossRef](#)]

32. Khurma, R.A.; Alsawalqah, H.; Aljarah, I.; Elaziz, M.A.; Damaševičius, R. An enhanced evolutionary software defect prediction method using island moth flame optimization. *Mathematics* **2021**, *9*, 1722. [[CrossRef](#)]
33. Wu, Z.; Shen, D.; Shang, M.; Qi, S. Parameter Identification of Single-Phase Inverter Based on Improved Moth Flame Optimization Algorithm. *Electr. Power Components Syst.* **2019**, *47*, 456–469. [[CrossRef](#)]
34. Rodríguez, J.; Bernet, S.; Wu, B.; Pontt, J.O.; Kouro, S. Multilevel voltage-source-converter topologies for industrial medium-voltage drives. *IEEE Trans. Ind. Electron.* **2007**, *54*, 2930–2945. [[CrossRef](#)]
35. Rodríguez, J.; Lai, J.S.; Fang, Z. Multilevel Inverters: A Survey of Topologies, Controls, and Applications. *IEEE Trans. Ind. Electron.* **2002**, *49*, 724–738. [[CrossRef](#)]
36. José, R.; Franquelo, L.G.; Samir, K.; León, J.I.; Portillo, R.C.; Prats, M.Á.M.; Pérez, M.A. Multilevel converters: An enabling technology for high-power applications. *Proc. IEEE* **2009**, *97*, 1786–1817. [[CrossRef](#)]
37. Allam, D.; Yousri, D.; Eteiba, M. Parameters extraction of the three diode model for the multi-crystalline solar cell/module using Moth-Flame Optimization Algorithm. *Energy Convers. Manag.* **2016**, *123*, 535–548. [[CrossRef](#)]
38. Li, Y.; Zhang, X.P.; Li, N. An Improved Hybrid PSO-TS Algorithm for Solving Nonlinear Equations of SHEPWM in Multilevel Inverters. *IEEE Access* **2022**, *10*, 48112–48125. [[CrossRef](#)]
39. Hiendro, A.; Yusuf, I.; Junaidi; Trias Pontia Wigyarianto, F.; Simanjuntak, Y.M. Optimization of SHEPWM cascaded multilevel inverter switching patterns. *Int. J. Power Electron. Drive Syst.* **2020**, *11*, 1570–1578. [[CrossRef](#)]
40. *IEEE Std 519-1992*; IEEE Recommended Practices and Requirements for Harmonic Control in Electrical Power Systems. IEEE: Piscataway, NJ, USA, 1993; pp. 1–101.

Disclaimer/Publisher's Note: The statements, opinions and data contained in all publications are solely those of the individual author(s) and contributor(s) and not of MDPI and/or the editor(s). MDPI and/or the editor(s) disclaim responsibility for any injury to people or property resulting from any ideas, methods, instructions or products referred to in the content.